

Chapter 8

Solar–Chemical Energy Conversion by Photocatalysis

Lan Yuan, Nan Zhang, Yi-Jun Xu, and Juan Carlos Colmenares

Abstract With the late but fast development, photocatalytic selective organic transformation has been recognized to be a promising alternative to traditional organic synthesis because it features unique advantages of being able to employ mild reaction conditions and avoid environmentally detrimental heavy metal catalysts as well as strong chemical oxidants or reducing agents. Moreover, it can facilitate the design of short and efficient reaction sequences, minimizing side processes and leading to high selectivity. This chapter provides an overview of the basic principles and evaluation methods of photocatalytic selective organic transformations. Recent progress on photocatalytic selective oxidation, reduction, and coupling reactions is represented based on selected examples. Besides, the future research challenges are concisely discussed.

Keywords Photocatalytic • Organic synthesis • Selective oxidation • Selective reduction • Coupling reactions

8.1 Introduction

Since the Industrial Age beginning with the invention of the steam engine in the 1760s, human beings have been exploiting fossil resources for energy and development. However, after more than 150 years' exploitation and utilization, expected depletion of the fossil fuel reserves has emphasized the issue of energy and environmental

L. Yuan • N. Zhang

State Key Laboratory of Photocatalysis on Energy and Environment, College of Chemistry, Fuzhou University, Fuzhou 350002, China

College of Chemistry, New Campus, Fuzhou University, Fuzhou 350108, People's Republic of China

Y.-J. Xu (✉)

State Key Laboratory of Photocatalysis on Energy and Environment, Fuzhou University, Industry Road 523, Fuzhou 350002, China

e-mail: yjxu@fzu.edu.cn

J.C. Colmenares (✉)

Institute of Physical Chemistry, Polish Academy of Sciences, ul. Kasprzaka 44/52, 01-224, Warsaw, Poland

e-mail: jcarloscolmenares@ichf.edu.pl

sustainability [1–6]. Heterogeneous photocatalysis by semiconductors, as a green technology, has received intense attention and been widely applied to environmental remediation and solar–chemical conversion for further energy supplies, including photodegradation of organic contaminants, photocatalytic CO₂ reduction for value-added chemicals, and water splitting for H₂ production [1, 2, 7–25].

The application of photocatalysis in selective organic transformations is not common at first because semiconductor photocatalysis has long been considered as “nonselective” processes, especially in aqueous media [26]. Nevertheless, many researchers have devoted efforts to this subject and have clarified that several reactions can proceed highly efficiently and selectively in various heterogeneous photocatalytic systems [26–32]. Following that, photocatalytic selective organic transformations have received growing interest and been recognized as an alternative to conventional synthetic routes for synthesis of fine chemicals through the selection of appropriate semiconductors and control of the reaction conditions [26, 27, 33–37]. Compared to traditional synthesis methods [34, 38–40], photocatalytic organic synthesis features several unique advantages: (i) it is driven by sunlight as a completely renewable source of energy; (ii) it can go on under milder conditions (room temperature and atmospheric pressure) and avoid environmentally detrimental heavy metal catalysts as well as strong chemical oxidants or reducing agents; (iii) it can facilitate the design of short and efficient reaction sequences, minimizing side processes and leading to high selectivity [29, 32–34, 38–42].

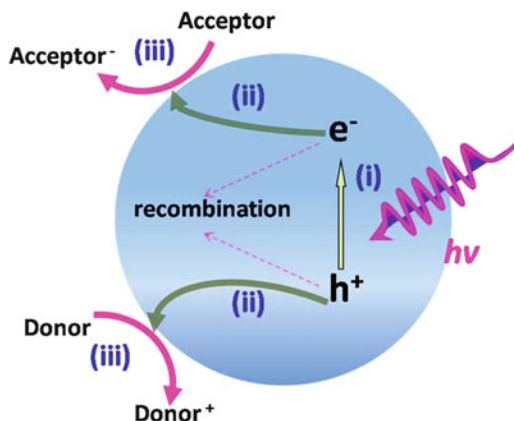
With the late but fast development, photocatalytic selective organic transformations have been considered to play a major role in promoting the evolution of twenty-first-century chemistry by replacing environmentally hazardous processes with environmental friendly and energy-efficient routes, allowing maximization of the quantity of raw material that ends up in the final product [26–34, 41, 43, 44]. To date, several organic transformation reactions are promoted with high selectivity and efficiency on various photocatalytic systems [26, 29–34, 38–41, 43–45]. This chapter will provide an overview of the basic principles and evaluation methods of photocatalytic selective organic transformations, following which recent progress in the significant examples of photocatalytic processes employed for synthetic purposes will be represented, including selective oxidation, reduction, and coupling reactions. In addition, the future research challenges will be concisely discussed.

8.2 Main Process and Basic Principles for Photocatalytic Selective Organic Transformations

In general, semiconductor-based photocatalytic process involves three main steps, as shown in Fig. 8.1, and the conversion of light into chemical energy by selective organic transformations can be described as $A + D = A_{\text{red}} + D_{\text{ox}}$. The optimization of every step plays an important role in boosting the photocatalytic efficiency.

Specifically, (i) upon light irradiation, the photocatalyst absorbs supra-bandgap photons ($\geq E_g$, Eq. 8.1), and photoexcited electron (e^-) and hole (h^+) pairs are produced in the CB and the VB, respectively (Eqs. 8.2 and 8.3). In this step, the

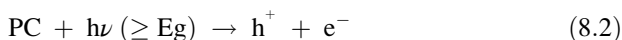
Fig. 8.1 Schematic illustration of semiconductor-based photocatalytic processes

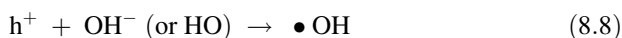


light absorption range and coefficient of photocatalyst should be increased to maximize the light harvesting and thus to harness more photons. In addition, since UV light only accounts for about 4 % of solar spectrum, it is highly desired for a photocatalyst with a narrow bandgap to utilize visible light, which occupies about 43 % of solar light [10, 46]. (ii) The photogenerated electrons and holes are separated and migrated to catalytically active sites at semiconductor surface (or recombined). Typically, photogenerated electron–hole pairs have a recombination time on the order of 10^{-9} s, while the chemical interaction with adsorbed species has a longer time of 10^{-8} – 10^{-3} s [46]. Therefore, in this step, accelerating the separation and migration of the photoexcited electrons and holes to avoid their recombination is fundamentally important. (iii) An efficient charge separation of the electron–hole pairs allows the respective oxidation and reduction reactions on the particle surface (Eqs. 8.4 and 8.5).

However, undesirable reactions might occur. On one hand, efficient back electron transfer between the primary redox products (Eq. 8.6) will prevent in most cases successive reactions to generate the final redox products. In this regard, efficient photocatalytic systems that can inhibit charge recombination as well as photocatalysts with proper electronic band structure for visible light harvesting and redox reactions are needed.

$$\text{Band gap (eV)} = \frac{1240}{\lambda(\text{nm})} \quad (8.1)$$





On the other hand, under most circumstances, molecular oxygen (O_2) usually functions as an electron acceptor by interacting with the photogenerated electrons on the CB of the photocatalyst, thus forming reactive oxygen species (ROS), superoxide radicals ($O_2^{\bullet -}$), an oxidizing agent (Eq. 8.7). In contrast, the holes on the VB react with surface hydroxyl groups or water molecules adsorbed on the surface of the photocatalyst and produce hydroxyl radicals, a different type of ROS acting as a strong oxidizing agent (Eq. 8.8). The ROS are highly nonselective oxidants and can degrade or completely oxidize the organic compounds all the way to the deep oxidation products to CO_2 and H_2O . Therefore, photocatalytic selective organic transformation to the desirable products by partially oxidizations is often hard to accomplish without the use of a proper electron or hole scavenger. Thus, using appropriate substrates and employing appropriate reaction conditions are of great importance for promoting selective organic transformations. That is, the type of electron-hole scavenger, the photocatalyst, the wavelength and the intensity of light used for irradiation, and the type of reactant and solvent all should be carefully chosen to achieve desired products.

8.3 Efficiency Evaluation of Photocatalytic Selective Organic Transformations

8.3.1 Light-Based Measures

The overall quantum yield and (apparent) quantum yield of photocatalytic process are defined in Eqs. 8.9 and 8.10, respectively:

$$\text{Overall quantum yield (\%)} = \frac{\text{Number of reacted electrons}}{\text{Number of absorbed photons}} \times 100\% \quad (8.9)$$

$$\text{(Apparent) quantum yield (\%)} = \frac{\text{Number of reacted electrons}}{\text{Number of incident photons}} \times 100\% \quad (8.10)$$

Based on the two equations, it is estimated that the apparent quantum yield should be smaller than the total quantum yield because not all the incident photons can be absorbed. However, this method is not often applied to evaluate selective organic transformations since the “number of reacted electrons” for these selective redox reactions is often difficult to be exactly determined, particularly for selective oxidation reactions, due to the relatively complex reaction process and

mechanisms. For example, regarding selective oxidation reactions, both the photogenerated holes and O_2 or activated oxygen (e.g., $\bullet O_2^-$ obtained by accepting the photogenerated electrons) can play the role in oxidizing the substrates.

8.3.2 Product-Based Measures

The most widely employed measure to evaluate the activity of photocatalytic selective organic transformations is the conversion, yield, and selectivity of the organic compounds transformed to target product. The definitions are as follows:

$$\begin{aligned}\text{conversion}(\%) &= [(C_0 - C_r)/C_0] \times 100 \\ \text{yield}(\%) &= C_p/C_0 \times 100 \\ \text{selectivity}(\%) &= [C_p(C_0 - C_r)] \times 100\end{aligned}$$

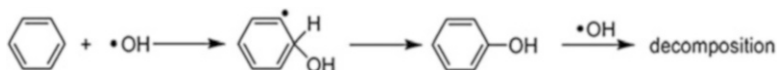
where C_0 is the initial concentration of reactant and C_r and C_p are the concentration of reactant and product at a certain time after the photocatalytic reaction, respectively.

8.4 Photooxidation of Organic Substrates

Oxidation processes play an important role in the production of a wide range of chemicals, where traditional industrial oxidation processes always need stringent reaction conditions and strong oxidants such as mineral acids, chromates, permanganate, hydrogen peroxide, etc [3, 28, 35, 47, 48]. Photooxidation can be cogitated as a possible alternative approach to overcome the harsh conditions as well as the questions of toxicity and corrosiveness.

8.4.1 Hydroxylation of Benzene

Phenol is an important industrial chemical because of its wide usage, ranging from disinfectant, precursor of phenolic resins to preservative for pharmaceutical aid [27, 49–56]. Different from the industrial production of phenol from benzene by the multistep cumene process under high temperature and pressure [57], photocatalytic hydroxylation of benzene to phenol can be realized via direct electrophilic addition of hydroxyl radicals ($\bullet OH$) under mild reaction conditions, since $\bullet OH$ can be generated through the reaction of the photogenerated holes from semiconductor photocatalysts with surface $-OH$ groups or adsorbed H_2O molecules. However, the product selectivity is often low since $\bullet OH$ is highly reactive and nonselective with hydroxylated phenols being further oxidized and mineralized. For example, the



Scheme 8.1 Photocatalytic oxidation of benzene to phenol and subsequent decomposition of phenol on TiO_2 (Reproduced with permission [26]. Copyright 2008 Elsevier)

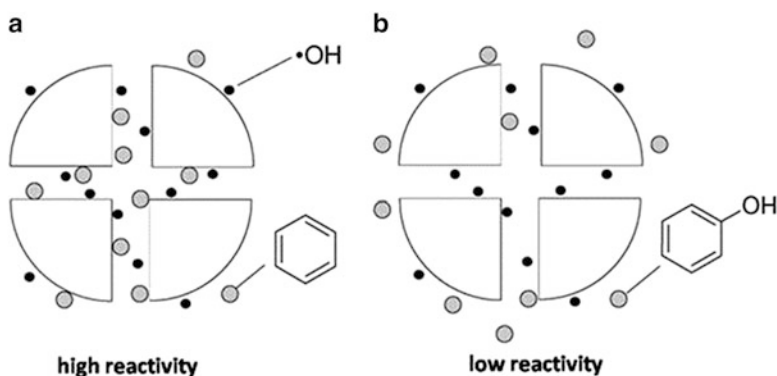


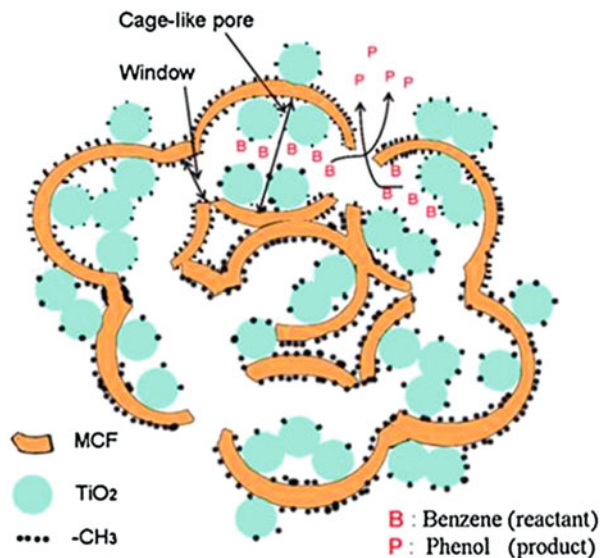
Fig. 8.2 Schematic representation of the reactivity difference between (a) benzene and (b) phenol on $m\text{TiO}_2$ (Reproduced with permission [26]. Copyright 2008 Elsevier)

photocatalytic oxidation of benzene to phenol with TiO_2 in aqueous media has been performed by many researchers [51–54, 56]. As shown in Scheme 8.1, the phenol produced by direct hydroxylation of benzene via an electrophilic addition of $\bullet\text{OH}$ radical formed on the TiO_2 surface can be sequentially decomposed by further reaction with $\bullet\text{OH}$ radicals [58–60] and results in a low phenol selectivity.

Therefore, efforts have been devoted to lower the affinity of phenol on the catalyst surface and thus reduce the possibility of further decomposition and improve the selectivity of phenol. For example, Skirmish's group has reported a system of mesoporous TiO_2 particles ($m\text{TiO}_2$) with high phenol selectivity (>80%) [56]. It is suggested that mesopores on the catalyst are the crucial factor for selective phenol production. As schematically shown in Fig. 8.2, benzene is a hydrophobic molecule and adsorbed well on the inner $m\text{TiO}_2$ surface, while hydrophilic phenol is scarcely adsorbed. The $\bullet\text{OH}$ radicals formed inside the pores scarcely diffuse out of the pores of $m\text{TiO}_2$ since they are deactivated rapidly in a near-diffusion controlled rate [27]. Therefore, they efficiently react with the well-adsorbed benzene, whereas less adsorbed phenol scarcely enters the pores and cannot react with them. In this way, further decomposition of phenol is effectively suppressed and high phenol selectivity is obtained.

Similarly, Choi's group later has reported a method for entrapping titanium oxide nanoparticles into hydrophobically modified mesocellular siliceous foam (MCF), which serves as an efficient photocatalyst for the selective hydroxylation of benzene to phenol. As shown in Fig. 8.3, the interior of the hydrophobically modified MCF (by surface organo-grafting with silylation agent) provides a

Fig. 8.3 Titanium oxide entrapped in the cage-like mesopores of hydrophobically modified mesocellular siliceous foam (MCF) for the hydroxylation of benzene (Reprinted with permission [51]. Copyright 2011 Elsevier)



hydrophobic environment where the reactant benzene molecules are preferentially attracted into mesopores, whereas the hydrophilic product phenol molecules are rapidly released out of the pores before they undergo further oxidative degradation within the MCF cages. Ultimately, the phenol selectivity is significantly enhanced [51].

In addition to the method of enhancing the catalytic performance of photocatalysts toward hydroxylation of benzene through improving their adsorption and desorption toward reactants and products specificity, efforts in terms of visible light harvesting have been devoted. For example, Huang and co-workers have prepared $M@TiO_2$ ($M = Au, Pt, Ag$) composites for direct oxidation of benzene to phenol in aqueous phenol under visible light irradiation, where $Au@TiO_2$ with a content of 2 wt% Au exhibits a high yield (63 %) and selectivity (91 %), as shown in Fig. 8.4a. The high photocatalytic activity for the composite is attributed to the enhanced visible light absorption as well as the strongest surface plasmon resonance (SPR) effect (Fig. 8.4b) [52]. Notably, the yield and selectivity of the phenol formation are increased with initially added phenol (ranging from 0 to 18,000 ppm) in water. As schematically shown in Fig. 8.4c, it is proposed that the initially added phenol is partially ionized into phenoxy anions and protons, and the SPR effect allows the electron transfer from the Au nanoparticle (NP) to the TiO_2 particle to which it is attached. Compared with benzene, the phenoxy anions are preferred to adsorb on electron-depleted Au NPs due to the opposite charges. Then, the electron-depleted Au NPs under visible light irradiation will oxidize phenoxy anions into phenoxy free radicals, which in turn oxidize benzene to phenol, thus becoming phenoxy anions again. Finally, O_2 dissolved in the solution is reduced by the electrons from the conduction band minimum (CBM) of TiO_2 . Increasing the

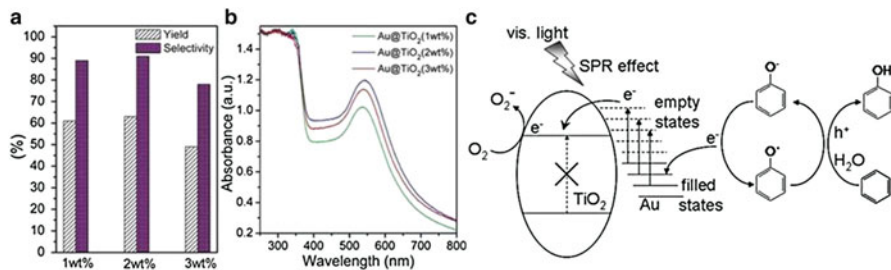


Fig. 8.4 (a) Visible light-induced catalytic oxidation of benzene with Au@TiO₂-microsphere composites with 1–3 wt% of Au. (b) UV/Vis diffuse-reflectance spectra of Au@TiO₂-microsphere composites. (c) Proposed mechanism for the photooxidation benzene into phenol in the presence of phenol under visible light irradiation (Reprinted with permission [52]. Copyright 2011 Royal Society of Chemistry)

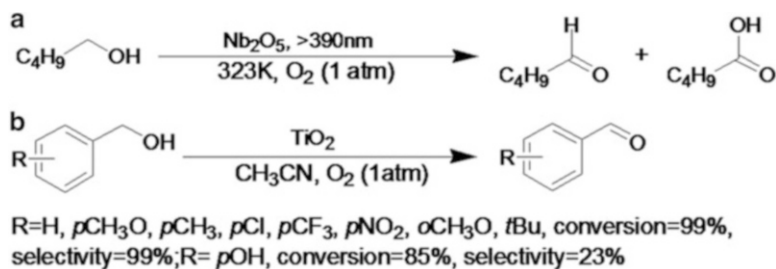
amount of initially added phenol will generate more phenoxy anions in water, which can lead to more phenoxy free radicals under visible light irradiation, thereby enhancing the oxidation of benzene.

Besides, Chen and co-workers have reported that Fe ion-modified porous graphitic carbon nitride (Fe-g-C₃N₄) is active for the direct oxidation of benzene to phenol in the presence of H₂O₂ at mild conditions (60 °C, 4 h) in both the presence (with a yield of 4.8 % based on benzene) and absence (with a yield of 1.8 % based on benzene) of visible light irradiation [55]. The enhanced yield of phenol with light irradiation is explained as that the surface-bound -Fe³⁺ can capture the photoinduced electrons, resulting in -Fe²⁺ to bind and reduce H₂O₂ to produce •OH, which is able to oxidize benzene to phenol. Moreover, when loading the Fe-g-C₃N₄ into the mesoporous system of SBA-15, the yield can be further improved to ~12 %, demonstrating that the activity is related to the exposure of the Fe-g-C₃N₄ surface structure and the increased surface active sites for benzene activation.

8.4.2 Oxidation of Alcohols

Selective oxidation of alcohols to carbonyls is a kind of rather important reactions both in industrial and laboratory synthesis since the products such as aldehydes and ketone derivatives are widely utilized in the fragrance, confectionary, and pharmaceutical industries [42, 61–63]. To date, photocatalytic selective oxidation of alcohols to the corresponding aldehydes and ketones has been performed both in liquid phase and gas phase. Since gas-phase reactions need high temperature, liquid-phase reactions are more appealing in the view of green chemistry. Moreover, its selectivity can be significantly improved by the deployment of organic solvent and visible light harvesting.

By weak bonding surface complexation of heteroatom (X=O, S, or N)-containing substrates, metal oxides (such as Nb₂O₅ and TiO₂) could

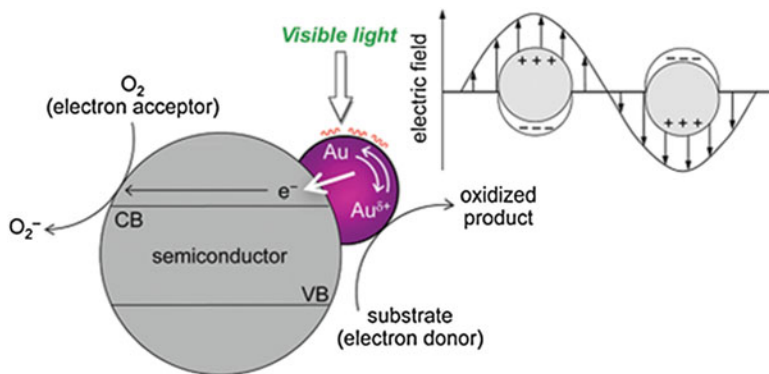


Scheme 8.2 (a) Photooxidation of 1-pentanol with Nb₂O₅ [64]. (b) Photooxidation of benzyl alcohol with various substitution groups with TiO₂ in CH₃CN [65, 66]

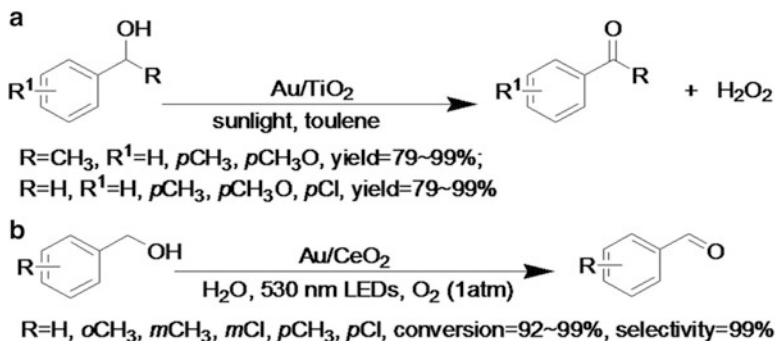
straightforwardly serve as the platform for visible light-induced organic reactions. For example, Shishido and co-workers have reported that the photooxidation of 1-pentanol can proceed over Nb₂O₅ under light irradiation (>390 nm), as shown in Scheme 8.2a [64]. The mechanism is proposed that alcohol is adsorbed onto Nb₂O₅ as an alcoholate species in the dark, which can be activated by visible light and transfer electrons to the conduction band reducing Nb⁵⁺ to Nb⁴⁺, resulting in the formation of the alcoholate species and a hydroxy group. And then the alcoholate species can be photoactivated to generate an alkenyl radical, which subsequently is converted to a carbonyl compound and desorbed, with the reduced Nb⁴⁺ sites reoxidized via the reaction with molecular oxygen.

Likewise, the oxidation of alcohols to corresponding carbonyl compounds with O₂ on anatase TiO₂ has been achieved under visible light irradiation (Scheme 8.2b) [65, 66]. It is proposed that the surface complexes formed by the interaction of the –CH₂OH group or possibly the phenyl ring of benzyl alcohol with the surface –OH group can induce absorption in the visible region [66]. Upon visible light irradiation, the surface complex is photoexcited to form holes (h⁺) and electrons (e[–]), and the holes can abstract hydrogen atoms from the –CH₂OH group of benzyl alcohol. Subsequently, the photoinduced benzyl alcoholic radicals may automatically release another electron to form benzaldehyde due to the current-doubling effect. Excellent conversion of 99 % and selectivity of 99 % are achieved for a series of substituted benzyl alcohols except when the substituent is –OH. This is because the substituted –OH group provides extra coordination sites for interacting with TiO₂, consequently leading to the destruction of the phenyl ring [67]. This mechanism is also applicable to rutile TiO₂ nanorods, which have been used for aerobic oxidation of benzyl alcohols to benzaldehydes, yielding a high selectivity of 99 % under visible light irradiation [68].

Localized surface plasmon resonance (SPR) arising from a resonant oscillation of free electrons coupled by light has been extensively studied and combined with semiconductors as promising heterogeneous photocatalysts because of their strong light absorption in the visible region. Tsukamoto et al. have prepared Au/TiO₂ via the deposition–precipitation method from H₄AuCl₄ and TiO₂ (Degussa, P25), which shows enhanced activity toward selective aerobic oxidation of alcohols relative to the reaction in the dark at room temperature [69]. It is proposed that



Scheme 8.3 Proposed mechanism for visible light-driven aerobic oxidation by Au particles supported on semiconductor particles (Reprinted with permission [69]. Copyright 2012 American Chemical Society)



Scheme 8.4 (a) Aerobic oxidation of alcohols with Au/TiO₂ in toluene under the irradiation of natural sunlight [69]. (b) Photooxidation of alcohols with various substitution groups with Au/CeO₂ [70]

for visible light-driven aerobic oxidation, as depicted in Scheme 8.3, plasmonic photocatalyst might oxidize a substrate (electron donor) on the Au surface, while e⁻ is consumed by the reduction of O₂ (electron acceptor) on the semiconductor surface. Besides, it is found that the catalyst architecture is critical for the activity, i.e., small Au particles ($d_{\text{Au}} < 5$ nm) loaded on P25 are necessary and Au particles located at the anatase/rutile interface behave as the active sites, facilitating efficient e⁻ transfer to TiO₂ and successful aerobic oxidation under sunlight irradiation, as shown in Scheme 8.4a. Apart from TiO₂, Kominami's group has prepared Au/CeO₂ by photochemical deposition of H₄AuCl₄ on CeO₂ in the presence of citric acid as the reducing agent, which presents the maximum absorption around 550 nm, in agreement with the SPR of Au NPs [70]. When exposed to 530 nm LED irradiation,

Table 8.1 Selective oxidation of a range of alcohols over the TiO₂-5 % GR photocatalyst under the visible light irradiation ($\lambda > 400$ nm) for 20 h (Reprinted with permission [72]. Copyright 2011 American Chemical Society)

Entry	Substrate	Product	Conversion (%)	Yield (%)	Selectivity (%)
1			62	62	100
2			70	70	100
3			80	80	100
4			74	73	99
5			45	43	96
6			84	76	91
7			50	46	92
8			41	37	90

benzyl alcohols can be stoichiometrically oxidized to corresponding benzaldehydes with O₂ in water, as displayed in Scheme 8.4b.

Our group has found that the introduction of graphene (GR) into semiconductors leads to enhanced performance for aerobic oxidation of various benzylic alcohols with different substituents and allylic alcohols [71–74]. As displayed in Table 8.1, GR-TiO₂ composite has been fabricated via a two-step wet chemistry approach, using graphene oxide (GO) and TiF₄ as the precursors of GR and TiO₂, respectively [72]. It is proposed that the superior and easily accessible “structure-directing” role of GO, the intimate interfacial contact between GR and TiO₂, and the better separation of the photogenerated carriers of GR-TiO₂ play a synergistic role in leading to the enhanced photocatalytic performance. Similarly, the introduction of GR into CdS substrate can also influence the morphology and structure, enhance the visible light absorption intensity, and improve the lifetime and transfer of photogenerated electron-hole pairs over the CdS-GR, leading to enhanced photocatalytic performance toward photocatalytic selective oxidation of benzylic and allylic alcohols, as shown in Fig. 8.5a [75]. In addition, it has been found the intimate interfacial interaction between CdS and GR can inhibit the photocorrosion of CdS during the photocatalytic reactions effectively.

In addition to the dual-ingredient hybrid systems, we have also constructed ternary nanocomposites with further improved photocatalytic performances toward

catalytic selective oxidation of alcohols, as shown in Fig. 8.5b [74]. Based on our previous CdS–GR composite with lamellar structure, TiO₂ nanoparticles can be uniformly carpeted on the surface of the CdS–GR by an in situ growth strategy [74]. The enhanced photocatalytic performance of ternary CdS–GR–TiO₂ hybrids can be ascribed to the combined interaction of larger surface area, the intimate interfacial contact among them, and two possible routes for electron transfer in the system [74]. The photogenerated electrons can transfer to the graphene nanosheets and TiO₂ simultaneously, which contributes to promoting the interfacial charge transfer rate and lengthening the lifetime of photogenerated electron–hole pairs, consequently resulting in the enhanced photoactivity.

Recently, our group has reported the transfer efficiency of photogenerated charge carriers across the interface between graphene (GR) and semiconductor CdS can be further improved by introducing a small amount of metal ions ($M = \text{Ca}^{2+}$, Cr^{3+} , Mn^{2+} , Fe^{2+} , Co^{2+} , Ni^{2+} , Cu^{2+} , and Zn^{2+}) as “mediator” into their interfacial layer matrix [73]. The photoactivity of GR–M–CdS for aerobic oxidation of alcohol is significantly improved (Fig. 8.5c) because the metal ions introduced can optimize the atomic charge carrier transfer pathway across the interface between GR and the semiconductor as well as drive a balance between the positive effect of GR on retarding the recombination of electron–hole pairs photogenerated from semiconductor and the negative “shielding effect” of GR resulting from the high weight addition of GR. Inspired by this, Pd has been selected as a typical noble metal to investigate whether it can play the similar role to metal ions as the interfacial mediator between GR and CdS. It is found that the ternary CdS–(GR–Pd)

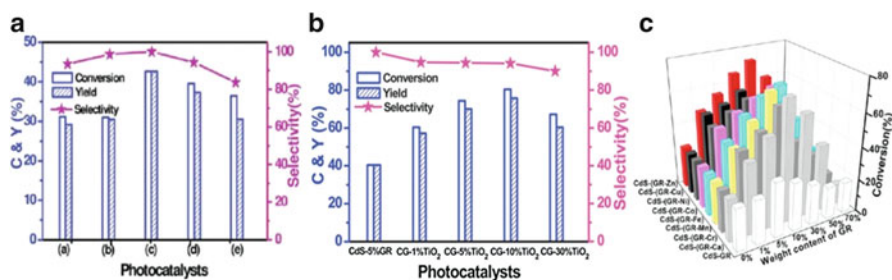


Fig. 8.5 (a) Photocatalytic selective oxidation of benzyl alcohol to benzaldehyde under the visible light irradiation over the as-prepared samples: (a) blank CdS; (b) CdS-1 % GR; (c) CdS-5 % GR; (d) CdS-10 % GR; and (e) CdS-30 % GR nanocomposites (Note: C and Y is short for conversion and yield. Reprinted with permission [75]. Copyright 2011 American Chemical Society). (b) CdS–GR–TiO₂ nanocomposites (Note: CG is short for CdS-5 % GR; GR–M–CdS nanocomposites. Reprinted with permission [74]. Copyright 2012 American Chemical Society). (c) Photocatalytic performance of blank CdS, CdS–GR, and CdS–(GR–M) ($M = \text{Ca}^{2+}$, Cr^{3+} , Mn^{2+} , Fe^{2+} , Co^{2+} , Ni^{2+} , Cu^{2+} , and Zn^{2+}) nanocomposites with different weight addition ratios of GR for photocatalytic selective oxidation of benzyl alcohol under visible light ($\lambda > 420 \text{ nm}$) for 2 h (Reprinted with permission [73]. Copyright 2014 American Chemical Society)

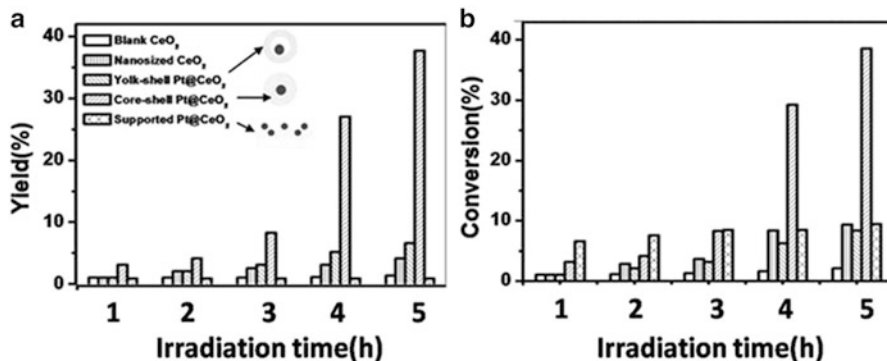


Fig. 8.6 The yield (a) and conversion (b) of photocatalytic selective oxidation of benzyl alcohol to benzaldehyde over the core-shell Pt/CeO₂, yolk-shell Pt/CeO₂, supported Pt/CeO₂, nanosized CeO₂ powder, and blank CeO₂ under the irradiation of visible light ($\lambda > 420$ nm) at room temperature and ambient atmosphere (Reprinted with permission [77]. Copyright 2011 Royal Society of Chemistry)

nanocomposite shows significantly enhanced visible light photocatalytic activity as compared to both blank CdS and the optimum binary CdS-GR, which verifies Pd can also play as the interfacial mediator to optimize and improve the spatial charge carrier separation and transfer across the interfacial domain between GR and CdS upon visible light irradiation [76].

Since optimizing the structure of the photocatalysts also has significant impact on the photocatalysts' performance, our group has synthesized the Pt/CeO₂ nanocomposite in an aqueous phase with tunable core-shell and yolk-shell structure via a facile and green template-free hydrothermal approach toward selective oxidation of benzyl alcohol [77]. The yield of benzaldehyde obtained over core-shell Pt/CeO₂ is ca. 9, 27, and 39 times higher than that of nanosized CeO₂, blank CeO₂, and supported Pt/CeO₂, respectively (Fig. 8.6), which can be ascribed to the advantageous core-shell structure, where Pt can trap/store the photogenerated electrons to prolong the lifetime of charge carriers, hence improving the efficiency toward photocatalytic redox process. As for the yolk-shell structure, the interfacial contact between the Pt core and CeO₂ shell is quite loose, and thus the role of Pt core has decreased markedly, resulting in lower photocatalytic activity.

In addition, Pd@CeO₂ semiconductor nanocomposite with "plum-pudding" structure has been fabricated via a facile low-temperature hydrothermal reaction of polyvinylpyrrolidone (PVP)-capped Pd colloidal particles and cerium chloride precursor followed by a calcination process in air, as shown in Fig. 8.7a [78]. This unique nanostructure endows the Pd@CeO₂ nanocomposite with enhanced activity and selectivity toward the visible light-driven oxidation of various benzylic alcohols to corresponding aldehydes using dioxygen as oxidant at room temperature and ambient pressure compared with a supported Pd/CeO₂ nanocomposite and nanosized CeO₂ powder (Fig. 8.7b, c), which is ascribed to the unique structure assembly of multi-Pd core@CeO₂ shell nanocomposite. First, the uniform structure

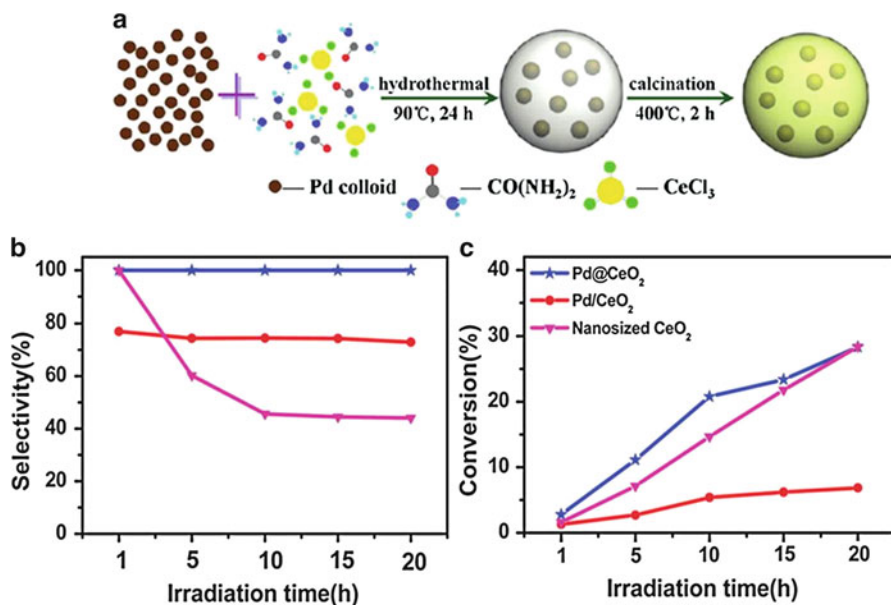


Fig. 8.7 Overall flowchart for fabrication of the multi-Pd core@ CeO_2 shell semiconductor nanocomposite (a); time-online photocatalytic selective oxidation of benzyl alcohol to benzaldehyde over the multi-Pd core@ CeO_2 shell nanocomposite, supported Pd/ CeO_2 , and commercial CeO_2 nanosized powder under the irradiation of visible light ($\lambda > 420$ nm) under ambient conditions, selectivity (b); conversion (c) (Reprinted with permission [78]. Copyright 2011 American Chemical Society)

composition, i.e., the evenly dispersed Pd cores are spatially encapsulated by the CeO_2 shell, provides a homogeneous environment for photocatalytic reaction. Second, the multi-Pd core@ CeO_2 shell nanostructure can significantly increase the surface area compared with the supported counterpart. Third, the “three-dimensional” intimate contact between the evenly dispersed Pd core and CeO_2 shell maximizes the metal–support interaction, which facilitates the interfacial charge transfer process.

Notably, aiming to give validity to targeted reactions for a fast screening of catalysts for photocatalytic transformations, Colmenares and co-workers have synthesized 24 different titania-based systems (either alone or modified with metals) through the sol–gel process varying the precursor (titanium isopropoxide or tetrachloride) and the aging (magnetic stirring, ultrasounds, microwave, or reflux) conditions. They are tested for liquid-phase selective photooxidation of 2-butenol (crotyl alcohol) to 2-butenal (crotonaldehyde) and gas-phase selective photooxidation of 2-propanol to acetone [61]. It is found that both test reactions (despite having very different reactant/catalyst ratio and contact times) show quite similar results in terms of influence of the precursor and the metals. That is, taking titanium isopropoxide as the precursor of titanium leads to better results than titanium tetrachloride and the presence of iron, palladium, or zinc is detrimental

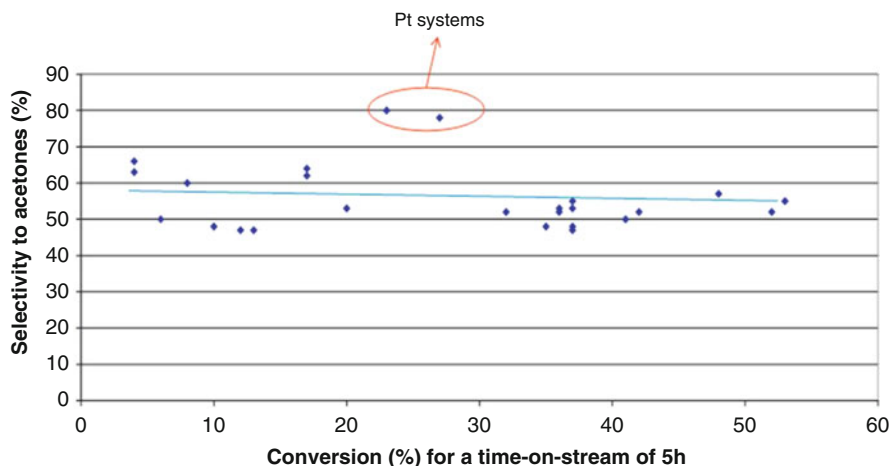


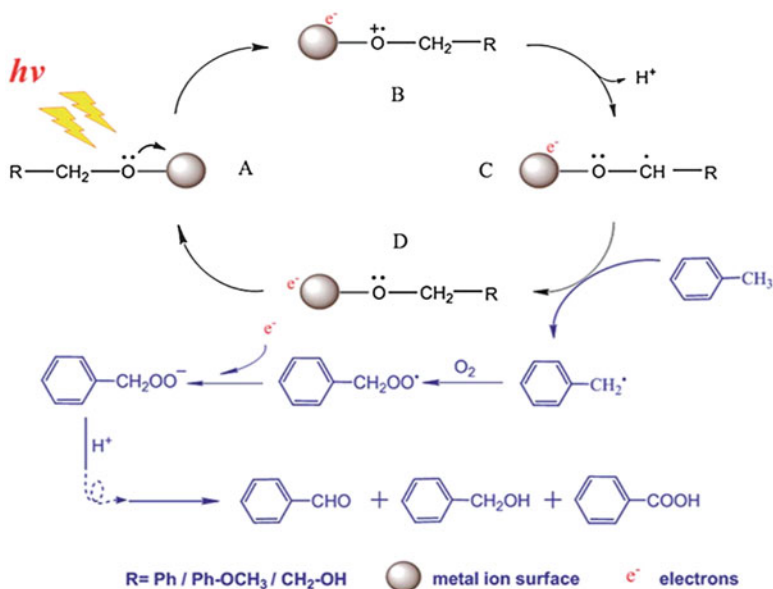
Fig. 8.8 Dependence of selectivity to acetone on 2-propanol conversion for all the titania-based systems used in the present study. Highlighted values correspond to platinum-containing titania (Reprinted with permission [61]. Copyright 2012 Elsevier)

to activity, whereas zirconium and especially gold can improve the results as compared to pure titania. Especially, for 2-propanol transformation into acetone, platinum-containing catalyst shows quite high selectivity values to acetone (in the 78–80 % range at 22–28 % conversion), suggesting that this test reaction is more sensitive to platinum, as shown in Fig. 8.8.

8.4.3 Oxidation of Saturated Primary C–H Bonds

The selective oxidation of stable alkyl aromatics such as toluene to commercial chemicals, including benzaldehyde, benzyl alcohol, benzoic acid, and benzyl benzoate with molecular oxygen, has important applications in fine chemicals and pharmaceutical production [79]. However, selective oxidation of C–H bonds with environmentally benign oxygen is often very difficult to control due to the abundance and inertness of C–H bonds in organic substrates. On the other hand, in thermal heterogeneous catalysis, the activation of saturated sp^3 C–H bonds often requires transition metal nanoparticles as a catalyst and relatively harsh reaction conditions. The rapid progress in selective transformation by heterogeneous photocatalysis presents the possibility of the selective activation of saturated sp^3 C–H bonds using molecular oxygen as a benign oxidant and visible light under ambient conditions [80, 81].

Zhu and co-workers have devised a new class of photocatalysts, metal hydroxide nanoparticles grafted with alcohols, which can efficiently oxidize alkyl aromatic compounds with O_2 using visible or ultraviolet light or even sunlight to generate the corresponding aldehydes, alcohols, and acids at ambient temperatures and give very



Scheme 8.5 Proposed pathways of the reaction mechanism for the selective oxidation of alkyl aromatics (Reprinted with permission [81]. Copyright 2012 Royal Society of Chemistry)

little overoxidation [81]. For example, toluene can be oxidized with a 23 % conversion after a 48 h exposure to sunlight with 85 % of the product being benzaldehyde and only a trace of CO₂. A tentative free radical mechanism is proposed, as shown in Scheme 8.5. The surface complexes catalyze the selective oxidation by an efficient mechanism that employs light absorption by the complexes to yield highly reactive surface radicals ($-\text{O}-\text{C}-\text{H}-\text{R}$), and these surface radicals initiate the aerobic oxidation of the organic molecules in contact with them. Moreover, the oxidation ability of the photocatalysts can be tuned through selection of the metal element and the alcohols grafted.

Our group has reported a cubic phase CdS semiconductor with specific sheet structure morphology synthesized by a simple room temperature method, which is able to be used as a visible light-driven photocatalyst for the selective oxidation of saturated primary C–H bonds in alkyl aromatics with high activity and selectivity using molecular oxygen as a benign oxidant and benzotrifluoride as the solvent under ambient conditions [82]. The superior photocatalytic performance of CdS is attributed to its unique structure assembly of specific sheet morphology with cubic phase, high surface area, and efficient separation of photogenerated charge carriers upon visible light irradiation. This work strongly suggests that tuning the microscopic structure and composition in diverse respects, e.g., size, shape, phase, crystallinity, or morphology, continues to be a very versatile, feasible, and general strategy to adjust the photocatalytic performance of a specific semiconductor photocatalyst with tunable photoactivity.

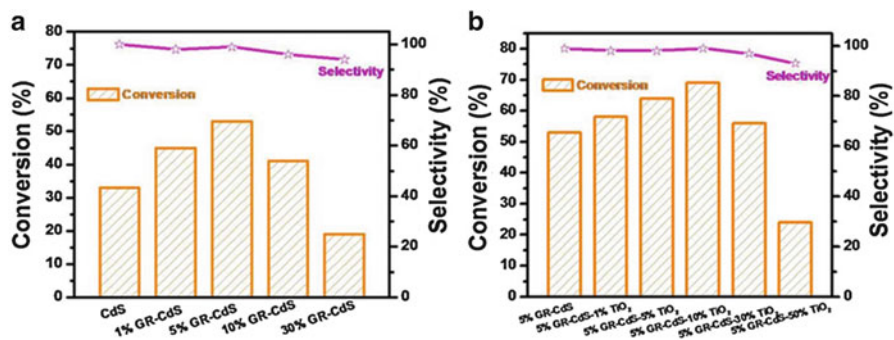
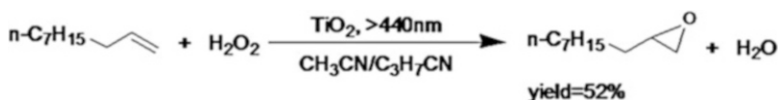


Fig. 8.9 Photocatalytic selective oxidation of toluene to benzaldehyde under visible light irradiation of 10 h over the as-prepared GR–CdS composites and blank CdS (a) and over GR–CdS–TiO₂ composites (b) (Reprinted with permission [83]. Copyright 2013 Nature Publishing Group)

Considering the fact that there is still a need to improve the photocatalytic performance of CdS for selective oxidation of C–H bonds, we later have designed and synthesized ternary GR–CdS–TiO₂ composites with an intimate spatial integration and sheetlike structure, which is afforded by assembling two co-catalysts, graphene and TiO₂, into the semiconductor CdS matrix with specific morphology as a visible light harvester [83]. As shown in Fig. 8.9, under visible light irradiation of 10 h, 53 % conversion of toluene is achieved over the optimal 5 % GR–CdS composite, which is much higher than 33 % conversion over the blank-CdS photocatalyst with the selectivity still maintained as high as 99 % (Fig. 8.9a). With the addition of second co-catalyst TiO₂, the photoactivity toward aerobic oxidation of C–H in toluene is further enhanced as compared to the binary 5% GR–CdS composite (Fig. 8.9b). It is proposed that the co-catalysts are able to cooperate with the light harvester to facilitate the charge separation/transfer and lengthen the lifetime of photogenerated electron–hole pairs, thereby resulting in an enhanced overall photocatalytic performance. This work demonstrates a wide, promising scope of adopting co-catalyst strategy to design more efficient semiconductor-based photocatalyst toward selective activation of C–H bonds using solar light and molecular oxygen.

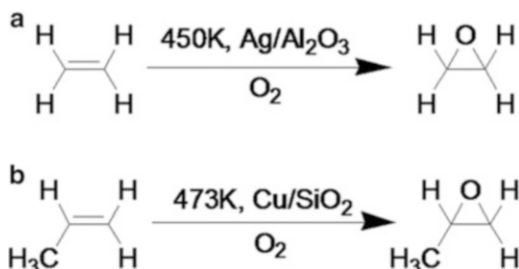
8.4.4 Epoxidation of Alkenes

The epoxidation of alkene is another type of reaction of industrial importance. However, since alkenes lack the suitable coordination sites present in heteroatom substrates, the weak adsorbed alkene substrates are unable to interact with TiO₂ directly to induce visible light absorbance. Thus, the deployment of H₂O₂ as the terminal oxidant is needed to form active surface complex through the interplay between H₂O₂ and TiO₂. As early as 2001, it is reported that 1-decene can be converted to 1,2-epoxydecane on TiO₂ powder using molecular oxygen as the



Scheme 8.6 Epoxidation of 1-decen to 1,2-epoxydecane with TiO_2 in $\text{CH}_3\text{CN}/\text{C}_3\text{H}_7\text{CN}$ [84]

Scheme 8.7 Epoxidation of ethylene to ethylene oxide (a) [85] and propylene to propylene oxide (b) [86]



oxygen source under UV light irradiation [84]. For rutile TiO_2 powders, the rate of epoxide generation can be significantly increased by addition of hydrogen peroxide (Scheme 8.6). In this case, the reaction can occur under visible light as well as UV light. The selectivity of the production of 1, 2-epoxydecane is higher under visible light than under UV light, due to the formation of $\text{Ti}\text{-}\eta^2\text{-peroxide}$ species on the surface of rutile TiO_2 upon treatment with H_2O_2 , which can induce visible light absorbance [84].

With regard to the plasmonic photocatalysts, Linic and co-workers have found that Ag nanocubes of ~60 nm edge length supported on $\alpha\text{-Al}_2\text{O}_3$ can be used for selective oxidation of ethylene to ethylene oxide (Scheme 8.7a) [85]. At 450 K, with the introduction of visible light into the system, the steady-state oxidation rate shows a fourfold increase relative to that driven by thermal energy only. And it is verified that the dissociation of molecular O_2 on silver to form adsorbed atomic oxygen controls the reaction rates. Later, they reported that Cu nanoparticles (NPs) with an average size of 41 nm supported on the inert SiO_2 (Cu/SiO_2) can tune the selectivity for the light-driven epoxidation of propylene to propylene oxide (Scheme 8.7b) [86]. The selectivity enhancement by Xe lamp irradiation is attributed to the localized SPR of Cu NPs which weakens the $\text{Cu}\text{-O}$ bond, thereby prompting the reduction of Cu_2O to Cu^0 .

Our group has reported an organic dye-like macromolecular “photosensitizer” role of graphene (GR) in wide-bandgap ZnS semiconductors for aerobic epoxidation of alkenes, including styrene, cyclohexene, and cyclooctene by visible light [87]. In this study, the assembly of nanosized ZnS particles on the two-dimensional platform of GR with an intimate interfacial contact has been prepared by a facile two-step wet chemistry process. Although the introduction of GR into the substrate of ZnS is not able to narrow the bandgap of ZnS to visible light region, the as-prepared ZnS-GR exhibits visible light photoactivity toward visible light irradiation ($\lambda > 420$ nm). Different from previous studies on GR-semiconductor

photocatalysts, where GR is claimed to behave as an electron reservoir to capture and shuttle the electrons photogenerated from the semiconductor, it is proposed that the GR in the ZnS–GR nanocomposites is serving as an organic dye-like macromolecular “photosensitizer.” Under visible light irradiation, GR is excited from the ground state to the excited state GR* and then injects electrons into the conduction band of ZnS, ultimately leading to visible light photoactivity.

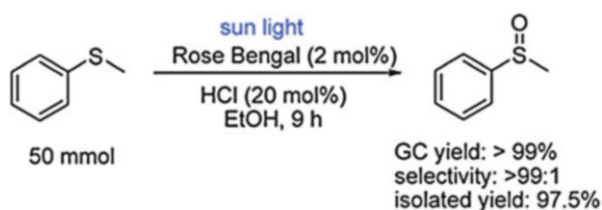
8.4.5 Sulfoxidation of Thioethers

The sulfoxidation of sulfides is important organic transformations in many fields, including pharmaceuticals, fossil fuel desulfurization, industrial wastewater treatment, and chemical warfare agent disposal [47, 88]. However, the over-sulfoxidation of sulfides into sulfone is the main side reaction, and efforts should be devoted to achieve selective sulfoxidation [89]. Photocatalytic sulfoxidation using molecular oxygen as the terminal oxidant turns out to be more advantageous toward achieving sustainable chemistry. Although the mechanism of sulfoxidation by molecular oxygen via photochemical irradiation has been investigated in physical chemistry [90–94], the applications are just beginning to be reported recently [48, 95–98].

Yao’s group has reported a metal-free aerobic selective sulfoxidation photosensitized by Rose Bengal (an organic dye) or solid-supported Rose Bengal, utilizing visible light as the driving force and molecular oxygen as the oxidant (Scheme 8.8) [97]. With the assistance of a catalytic amount of hydrochloric acid, Rose Bengal appears to be the most efficient and selective catalyst toward the selective sulfoxidation of thioanisole, compared to the metal complex photoredox catalysts. A series of other thioethers have been subjected to the optimized reaction conditions, verifying the generality of this reaction. In addition, Rose Bengal is readily accessible and inexpensive, and with the use of a solid-support catalyst, the workup procedure can be significantly improved. Moreover, a 50 mmol scale reaction has been carried out in an Erlenmeyer flask under sunlight on the roof of the chemistry building and demonstrated that the reaction is practical and scalable.

Apart from various organic photocatalysts, our group has reported a spatially branched hierarchical system composed of inorganic photocatalysts, CdS/ZnO nanocomposites (CZ), and its photoactivity toward sulfoxidation of thioanisole has been tested (Fig. 8.10) [99]. The conversion for thioanisole and yield for

Scheme 8.8 Selective sulfoxidation of thioanisole under sunlight with Rose Bengal (Reprinted with permission [97]. Copyright 2013 Royal Society of Chemistry)



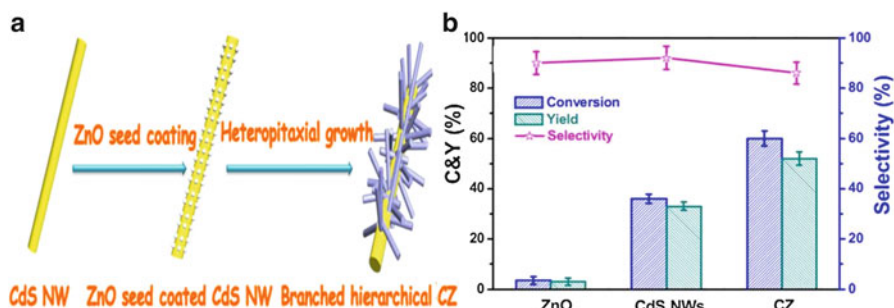
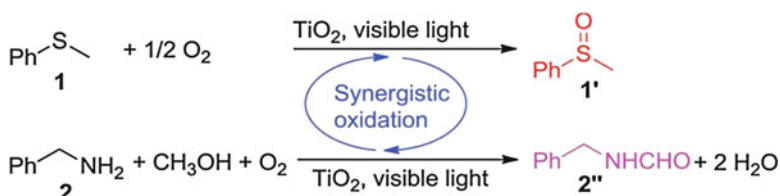


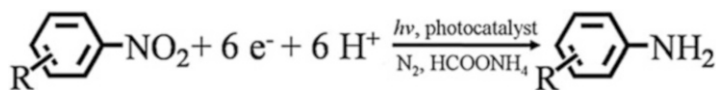
Fig. 8.10 (a) Schematic illustration for synthesis of branched hierarchical CZ nanocomposites and (b) photocatalytic performance of CdS NWs, blank ZnO, and branched hierarchical CZ nanocomposites for selective oxidation of thioanisole (Reprinted with permission [99]. Copyright 2014 Royal Society of Chemistry)



Scheme 8.9 The synergistic aerobic oxidation of two substrates, sulfide **1** and amine **2**, occurs simultaneously on the surface of TiO_2 under visible light irradiation (Reprinted with permission [95]. Copyright 2015 Royal Society of Chemistry)

methylsulfanylbenzene are about 60 % and 52 % over the branched hierarchical CZ, respectively, which are much higher than the values obtained over CdS NWs (conversion 36 % and yield 33 %) and blank ZnO (conversion 3.5 % and yield 3 %). The enhanced photoactivities can be ascribed to the branched hierarchical structure of CZ nanocomposites, which can not only increase the light harvesting efficiency but also boost charge separation and faster charge transport and collection. Additionally, under light irradiation, the branched hierarchical CZ nanocomposites are thought to generate a “Z-scheme” system [7] to drive the photocatalytic processes.

Recently, Zhao and co-workers have achieved the selective oxidation of thioanisole with TiO_2 photocatalyst under visible light irradiation by combining the aerobic oxidation of sulfide and the aerobic oxidative formylation of amine with methanol through the synergistic interplay of reactants and catalyst (Scheme 8.9) [95]. In contrast, attempts to perform these two reactions individually are not successful. The mechanism for the selective synergistic aerobic oxidation of thioanisole **1** and benzylamine **2** has been proposed and demonstrated in Scheme 8.10. The adsorption of benzylamine on TiO_2 leads to the formation of surface complex **a**, which shows activity under visible light irradiation, facilitating



Scheme 8.11 Photocatalytic reduction of nitro compounds to amino compounds in water with the addition of ammonium formate (HCOONH_4) for quenching photogenerated holes under N_2 atmosphere

irradiation ($\lambda = 365 \text{ nm}$) of 4-nitrophenol in methanol suspensions. It is proposed that the photoreduction rate is significantly affected by the solvent parameters, such as viscosity, polarity, and polarizability. For example, increase in the polarity parameter leads to better stabilization of the charged intermediate and accelerates the photocatalytic reduction.

Xu et al. have prepared GR-modified TiO_2 hybrids by electrostatic assembly, and its photocatalytic reduction of nitroaromatics to the corresponding aminoaromatics is examined under UV light irradiation [104]. When the dosage of GO is about 1.0 %, almost all of the 4-nitrophenol is converted, and the yield rate of 4-aminophenol achieves around 95 % with $\text{H}_2\text{C}_2\text{O}_4$ as hole scavenger under N_2 purge. The results indicate that the addition of GR can effectively minimize the recombination of photogenerated charge carriers derived from the irradiated TiO_2 and better encourage these separated electrons to participate in the reactions. In addition, it is found that different hole scavengers lead to discrepant reduction efficiency. Therefore, to adjust and optimize such photocatalytic reduction reactions is of great importance to improve its reduction ability.

Our group has fabricated various GR-based nanocomposites such as CdS nanowire/GR [100], CdS nanosphere/GR [105], $\text{In}_2\text{S}_3/\text{GR}$ [102], $\text{ZnIn}_2\text{S}_4/\text{GR}$ [106], TiO_2/CdS nanowire/GR [107], GR-M-CdS ($\text{M} = \text{Ca}^{2+}, \text{Cr}^{3+}, \text{Mn}^{2+}, \text{Fe}^{2+}, \text{Co}^{2+}, \text{Ni}^{2+}, \text{Cu}^{2+}, \text{and Zn}^{2+}$) [73], GR-Pd-CdS [76], and hierarchical CdS-ZnO-GR hybrids [108]. It is found that their photoactivities for reduction of nitro compounds to amino compounds with ammonium formate (HCOONH_4) for hole scavenger in N_2 atmosphere (Scheme 8.11) under visible light irradiation are all remarkably enhanced as compared to the blank semiconductors [73, 100–102, 106, 107]. It has been concluded that the selective reduction efficiency can be driven by appropriate introduction of GR into the matrix of pure semiconductor, which can boost the transfer and prolong the lifetime of the electrons photoexcited from the semiconductor due to the tighter connection between GR and the semiconductor, as well as the optimization of the atomic charge carrier transfer pathway across the interface between GR and the semiconductor.

In addition, our group has designed a Pd/ CeO_2 hollow core-shell nanocomposite (Pd@hCeO_2) composed of tiny Pd nanoparticle (NP) cores encapsulated within CeO_2 hollow shells, as shown in Fig. 8.11a [109]. As compared to supported Pd/ CeO_2 and commercial CeO_2 , the as-prepared Pd@hCeO_2 demonstrates improved photoactivity toward selective reduction of aromatic nitro compounds under visible light irradiation with the addition of ammonium oxalate as quencher for photogenerated holes and N_2 purge at room temperature (Table 8.2). It is

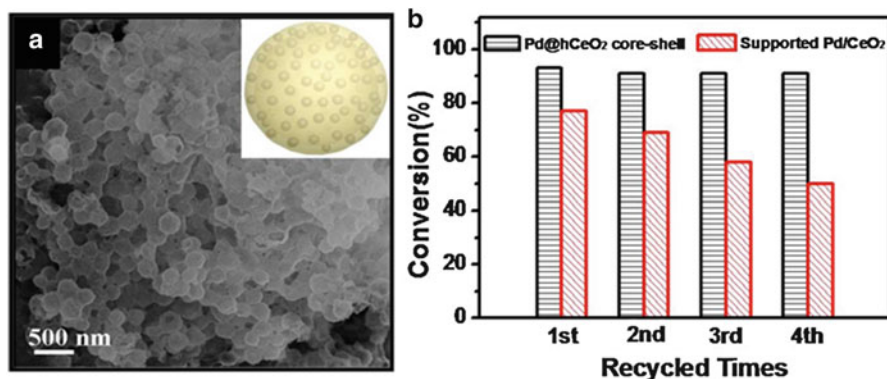


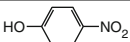
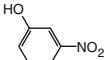
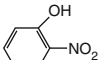

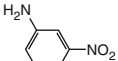
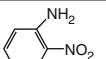
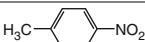
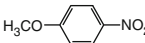
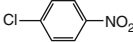

Fig. 8.11 (a) Typical SEM images of Pd@hCeO₂ core-shell nanocomposite. (b) Stability testing of photocatalytic activity of supported Pd/CeO₂ and Pd@hCeO₂ core-shell nanocomposites for reduction of 4-nitrophenol under visible light irradiation ($\lambda > 420$ nm) for 6 h (Reprinted with permission [109]. Copyright 2013 American Chemical Society)

recognized that the CeO₂ shell acts as the primary active component to give photogenerated electron-hole pairs, while the Pd nanoparticle cores with low-lying Fermi level serve as an electron reservoir to prolong the lifetime of the charge carriers. The three-dimensional interfacial contact between Pd cores and hollow CeO₂ shells facilitates the efficient charge carrier transfer, thereby leading to the enhanced fate of photogenerated electron-hole pairs from CeO₂. In particular, the core-shell strategy efficiently prevents the aggregation of Pd NPs in the high-temperature calcination process and the leaching of Pd NPs for the catalytic reaction in a liquid phase, which is not able to be achieved for traditional supported Pd/CeO₂ catalyst. As shown in Fig. 8.11b, the core-shell Pd@hCeO₂ almost does not have the loss of photoactivity during the recycled activity testing on reused samples, whereas the significant loss of photoactivity is clearly observed for supported Pd/CeO₂, due to the significant leaching of Pd nanoparticles in supported Pd/CeO₂.

8.6 Coupling Reactions

The photoinduced charge separation occurring on the surface of photocatalysts creates both a reduction center and an oxidation center. This unique feature allows multistep reactions on a single photocatalyst: intermediates generated from one reaction center could be the substrates at another center. The integrated use of both reaction centers could therefore complete a sophisticated multistep synthesis in “one-pot” reaction, i.e., the coupling reactions.

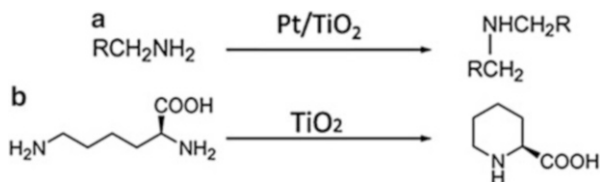
Table 8.2 Photocatalytic reduction of substituted aromatic nitro compounds over Pd@hCeO₂ core-shell nanocomposite, supported Pd/CeO₂, and commercial CeO₂ aqueous suspension under visible light irradiation ($\lambda > 420$ nm) with the addition of ammonium oxalate as quencher for photogenerated holes and N₂ purge at room temperature (Reprinted with permission [109]. Copyright 2013 American Chemical Society)

Entry	Substrate	t/[h]	Conversion (%)		
			Pd@hCeO ₂	Pd/CeO ₂	CeO ₂
1		6	93	77	19
2		6	87	69	16
3		6	99	81	22
4		6	64	44	13
5		6	50	35	8
6		6	43	22	6
7		4	96	75	14
8		6	84	55	11
9		4	92	75	17
10		4	94	73	15

8.6.1 C–N Coupling

Various kinds of organic compounds can be synthesized through C–N coupling reactions [110–112]. For example, Ohtani and co-workers have found that photoirradiation to an aqueous solution containing primary amines in the presence of a powdered mixture of TiO₂ with Pt black (Pt/TiO₂ catalyst) gives rise to the corresponding secondary amines via C–N coupling reaction (Scheme 8.12a) [113]. L-Pipecolinic acid has been achieved by the cyclization reaction through photoirradiation of a deaerated aqueous suspension of TiO₂ containing L-lysine (Scheme 8.12b). This reaction involves a single-electron transfer from the terminal amino group of L-pipecolinic acid to h⁺ on the TiO₂ surface and subsequent removal of the amino group, leading to intramolecular C–N coupling to form an imine, which is then reduced to form the L-pipecolinic acid. The highest selectivity (77 %) and conversion of L-lysine (90 %) have been achieved [110].

The C–N coupling reaction also can proceed between amines and alcohols. For example, photoirradiation to an alcohol solution containing primary or secondary amines with Pt/TiO₂ can produce the corresponding secondary or tertiary amines [114, 115]. In these reactions, alcohols are oxidized by h⁺ formed on the catalyst



Scheme 8.12 (a) Photocatalytic transformation of primary amines to secondary amines via C–N coupling reaction on Pt/TiO₂ [113]. (b) Photocatalytic transformation of L-lysine to L-pipecolinic acid via C–N coupling reaction on TiO₂ [110]

surface to the corresponding aldehydes or ketones, which then could couple with amine to form an imine. In addition, imines can also be produced by reacting alkynes with amines to hydro-amination products with Au nanoparticles supported on nitrogen-doped TiO₂ (Au/TiO₂–N), which serves as the visible light plasmonic photocatalyst [116]. The presence of Ti³⁺ of TiO₂, arising from nitrogen doping, provides more coordination sites for the alkyne, thereby prompting a better performance than that of pure TiO₂ (Scheme 8.13a). Through a similar reaction, propargyl-amines have been produced by a one-pot synthesis procedure with the introduction of aldehyde to the amine and alkyne mixture, on the catalyst Au/ZnO under 530 nm LED irradiation (Scheme 8.13b) [117]. The high yields of propargyl-amines result from the interaction of alkyne with the ZnO support. Therefore, the use of plasmonic photocatalysts can also be employed to manipulate the oxidative condensation of amine with aldehyde under visible light irradiation.

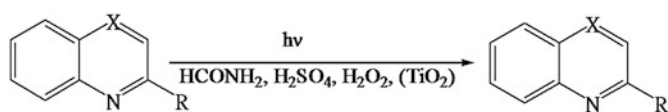
8.6.2 C–C Coupling

Heterocyclic bases can easily be functionalized via C–C coupling by the reaction with amides or ethers. For example, Caronna and co-workers have found that with the addition of H₂SO₄ and H₂O₂, heterocyclic bases can react with amide to produce the corresponding amide-functionalized heterocycles (Scheme 8.14) [118]. It is considered that during these reactions, amide first reacts with •OH radical formed on the TiO₂ surface to form amide radical via hydrogen abstraction, which then attacks the heterocyclic bases and produces the C–C coupling products. The additional H₂SO₄ and H₂O₂ can accelerate the amide radical formation.

Subsequently, it is reported by the same group that the reactions between various heterocyclic bases and ethers can be induced by sunlight, and various kinds of heterocycle-ether conjugates are formed in liquid–solid heterogeneous system in the presence of TiO₂ (Scheme 8.15) [119]. The derivatives obtained with trioxane may give an easy entry to heterocyclic aldehydes. It is considered that in these reactions, the α-oxyalkyl radical is generated by hydrogen abstraction from the α-carbon of the ethers or by electron transfer from the oxygen atom of the ethers, which then is claimed to attack the heterocyclic bases to form the heterocycle-ether conjugates.



Scheme 8.13 Photocatalytic C–N coupling reactions between alkynes with amines (Reprinted with permission [33]. Copyright 2014 Royal Society of Chemistry)



(1) X = CH, R = H

(2) X = CH, R = CH₃

(3) X = C-CH₃, R = H

(4) X = N, R = H

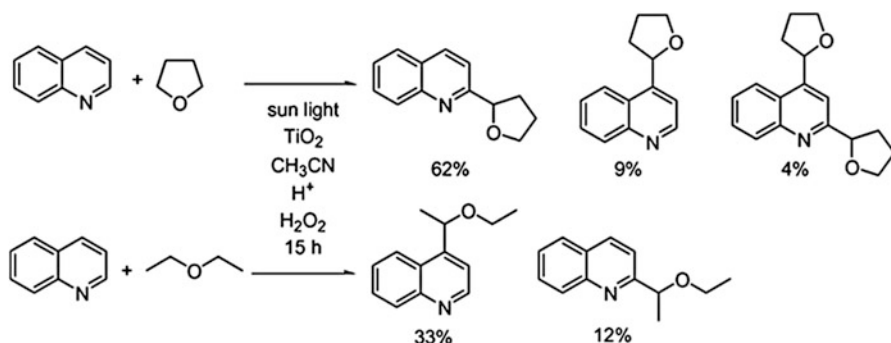
(5) X = CH, R = CONH₂

(6) X = C-CONH₂, R = CH₃

(7) X = C-CH₃, R = CONH₂

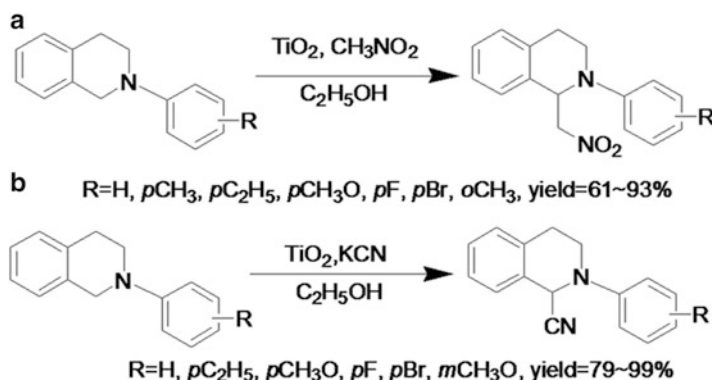
(8) X = N, R = CONH₂

Scheme 8.14 Photocatalytic reactions of heterocyclic bases and formamide in aqueous solution with TiO₂ (Reprinted with permission [118]. Copyright 2003 Royal Society of Chemistry)

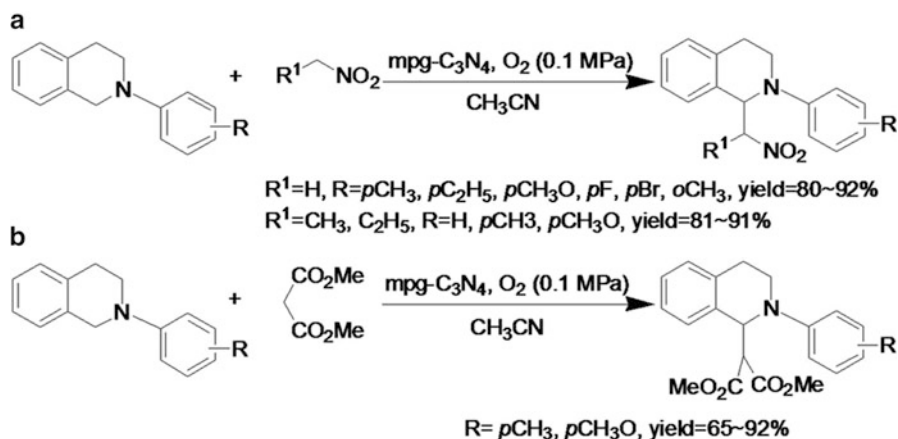


Scheme 8.15 Photocatalytic functionalization of heterocyclic base with ethers by TiO₂ (Reprinted with permission [26]. Copyright 2008 Elsevier)

In addition, other nucleophiles have also been incorporated into the activated substrates adjacent to N-atom, enabling even more complicated functionalization under visible light irradiation on P25 TiO₂. Using P25 as a photocatalyst, new C–



Scheme 8.16 C–C coupling of a variety of N-aryltetrahydroisoquinolines with CH_3NO_2 and KCN over TiO_2 (Reprinted with permission [33]. Copyright 2014 Royal Society of Chemistry)



Scheme 8.17 C–C coupling of a variety of N-aryltetrahydroisoquinolines with nitroalkanes and dimethyl malonate over $\text{mpg-C}_3\text{N}_4$ (Reprinted with permission [33]. Copyright 2014 Royal Society of Chemistry)

bonds were successfully constructed under the mild visible light irradiation of an 11 W fluorescent lamp [120]. As shown in Scheme 8.16, both CH_3NO_2 and KCN are able to act as the nucleophile to facilitate the formation of different C–C bonds to afford different tetrahydroisoquinoline derivatives in good to excellent yields [120].

Besides, Möhlmann and co-workers have operated $\text{mpg-C}_3\text{N}_4$ as a visible light photocatalyst to functionalize the benzylic C–H adjacent to N-atoms with a suitable nucleophile, using 0.1 MPa of O_2 as the oxidant, without the assistance of an additional additive. Under the visible light irradiation, a variety of N-aryltetrahydroisoquinolines could be connected with nitroalkanes and dimethyl malonate to construct new C–C bonds, as shown in Scheme 8.17 [121].

8.7 Conclusion

Selective organic transformation plays an important role in the synthesis of various commodity chemicals closely linked to our daily lives. In comparison to conventional methods, photocatalytic organic transformations possess several inherent advantages, including benign environmental impacts and employment of mild reaction conditions. It is offering an alternative “green” route for the production of organics. However, despite significant progress made in this area of research as reviewed above, typical challenges still exist and need to be resolved before it is more viable for large-scale practical applications. In this regard, more exciting discoveries of efficient photocatalysts and more precise deployment of the reaction conditions are required to be conceived in the pursuit of higher conversion and higher selectivity for photocatalytic organic transformations in a practical scale-up manner. More investigations are needed to deepen our understanding of the photo-induced interfacial charge carrier transfer processes and optimized photocatalytic reactor design, which can help effectively promote the development and implementation of rapid global spread of organic synthesis by semiconductor-based photocatalysis. Hopefully, because many organic reactions are thermodynamic downhill exothermic reactions, thus we believe that the prospect of photocatalytic organic transformations in practical application is more available.

Acknowledgments The support from the Key Project of National Natural Science Foundation of China (U1463204), the National Natural Science Foundation of China (20903023 and 21173045), the Award Program for Minjiang Scholar Professorship, the Natural Science Foundation of Fujian Province for Distinguished Young Investigator Grant (2012 J06003), the Independent Research Project of State Key Laboratory of Photocatalysis on Energy and Environment (NO. 2014A05), the first Program of Fujian Province for Top Creative Young Talents, and the Program for Returned High-Level Overseas Chinese Scholars of Fujian province is kindly acknowledged.

References

1. Ran J, Zhang J, Yu J, Jaroniec M, Qiao SZ (2014) Earth-abundant cocatalysts for semiconductor-based photocatalytic water splitting. *Chem Soc Rev* 43(22):7787–7812
2. Yang J, Wang D, Han H, Li C (2013) Roles of cocatalysts in photocatalysis and photoelectrocatalysis. *Acc Chem Res* 46(8):1900–1909
3. Chen X, Shen S, Guo L, Mao SS (2010) Semiconductor-based photocatalytic hydrogen generation. *Chem Rev* 110(11):6503–6570
4. Navarro Yerga RM, Álvarez Galván MC, Del Valle F, Villoria de la Mano JA, Fierro JL (2009) Water splitting on semiconductor catalysts under visible-light irradiation. *Chemsuschem* 2(6):471–485
5. Stott PA, Tett S, Jones G, Allen M, Mitchell J, Jenkins G (2000) External control of 20th century temperature by natural and anthropogenic forcings. *Science* 290(5499):2133–2137
6. Herzog HJ (2001) Peer reviewed: what future for carbon capture and sequestration? *Environ Sci Technol* 35(7):148A–153A
7. Zhou P, Yu J, Jaroniec M (2014) All-solid-state Z-scheme photocatalytic systems. *Adv Mater* 26(29):4920–4935

8. Wang C, Astruc D (2014) Nanogold plasmonic photocatalysis for organic synthesis and clean energy conversion. *Chem Soc Rev* 43(20):7188–7216
9. Tong H, Ouyang S, Bi Y, Umezawa N, Oshikiri M, Ye J (2012) Nano-photocatalytic materials: possibilities and challenges. *Adv Mater* 24(2):229–251
10. Shen S, Shi J, Guo P, Guo L (2011) Visible-light-driven photocatalytic water splitting on nanostructured semiconducting materials. *Int J Nanotechnol* 8(6):523–591
11. Maeda K (2011) Photocatalytic water splitting using semiconductor particles: history and recent developments. *J Photochem Photobiol C* 12(4):237–268
12. Langer R, Leitus G, Ben-David Y, Milstein D (2011) Efficient hydrogenation of ketones catalyzed by an iron pincer complex. *Angew Chem* 123(9):2168–2172
13. Navarro RM, Alvarez-Galvan MC, Villoria de la Mano JA, Al-Zahrani SM, Fierro JLG (2010) A framework for visible-light water splitting. *Energy Environ Sci* 3(12):1865–1882
14. Maeda K, Domen K (2010) Photocatalytic water splitting: recent progress and future challenges. *J Phys Chem Lett* 1(18):2655–2661
15. Tu W, Zhou Y, Zou Z (2014) Photocatalytic conversion of CO₂ into renewable hydrocarbon fuels: state-of-the-art accomplishment, challenges, and prospects. *Adv Mater* 26(27):4607–4626
16. Liu L, Li Y (2014) Understanding the reaction mechanism of photocatalytic reduction of CO₂ with H₂O on TiO₂-based photocatalysts: a review. *Aerosol Air Qual Res* 14(2):453–469
17. Li K, An X, Park KH, Khraisheh M, Tang J (2014) A critical review of CO₂ photoconversion: catalysts and reactors. *Catal Today* 224:3–12
18. Izumi Y (2013) Recent advances in the photocatalytic conversion of carbon dioxide to fuels with water and/or hydrogen using solar energy and beyond. *Coord Chem Rev* 257(1):171–186
19. Habisreutinger SN, Schmidt-Mende L, Stolarczyk JK (2013) Photocatalytic reduction of CO₂ on TiO₂ and other semiconductors. *Angew Chem Int Ed* 52(29):7372–7408
20. Mori K, Yamashita H, Anpo M (2012) Photocatalytic reduction of CO₂ with H₂O on various titanium oxide photocatalysts. *RSC Adv* 2(8):3165–3172
21. Liu G, Wang K, Hoivik N, Jakobsen H (2012) Progress on free-standing and flow-through TiO₂ nanotube membranes. *Sol Energy Mater Sol Cells* 98:24–38
22. Yui T, Tamaki Y, Sekizawa K, Ishitani O (2011) Photocatalytic reduction of CO₂: from molecules to semiconductors. *Photocatal* 303:151–184
23. Wu C, Zhou Y, Zou Z (2011) Research progress in photocatalytic conversion of CO₂ to hydrocarbons. *Chin J Catal* 32(10):1565–1572
24. Roy SC, Varghese OK, Paulose M, Grimes CA (2010) Toward solar fuels: photocatalytic conversion of carbon dioxide to hydrocarbons. *ACS Nano* 4(3):1259–1278
25. Jiang Z, Xiao T, Kuznetsov V, Edwards P (2010) Turning carbon dioxide into fuel. *Philos Trans R Soc A Math Phys Eng Sci* 368(1923):3343–3364
26. Shiraishi Y, Hirai T (2008) Selective organic transformations on titanium oxide-based photocatalysts. *J Photochem Photobiol C* 9(4):157–170
27. Lawless D, Serpone N, Meisel D (1991) Role of hydroxyl radicals and trapped holes in photocatalysis. A pulse radiolysis study. *J Phys Chem* 95(13):5166–5170
28. Fox MA, Dulay MT (1993) Heterogeneous photocatalysis. *Chem Rev* 93(1):341–357
29. Palmisano G, Augugliaro V, Pagliaro M, Palmisano L (2007) Photocatalysis: a promising route for 21st century organic chemistry. *Chem Commun* 33:3425–3437
30. Pratti S, Fagnoni M (2009) The sunny side of chemistry: green synthesis by solar light. *Photochem Photobiol Sci* 8(11):1499–1516
31. Ravelli D, Dondi D, Fagnoni M, Albini A (2009) Photocatalysis. A multi-faceted concept for green chemistry. *Chem Soc Rev* 38(7):1999–2011
32. Palmisano G, García-López E, Marci G, Loddo V, Yurdakal S, Augugliaro V, Palmisano L (2010) Advances in selective conversions by heterogeneous photocatalysis. *Chem Commun* 46(38):7074–7089

33. Lang X, Chen X, Zhao J (2014) Heterogeneous visible light photocatalysis for selective organic transformations. *Chem Soc Rev* 43(1):473–486
34. Yang M-Q, Xu Y-J (2013) Selective photoredox using graphene-based composite photocatalysts. *Phys Chem Chem Phys* 15(44):19102–19118
35. Colmenares JC, Luque R (2014) Heterogeneous photocatalytic nanomaterials: prospects and challenges in selective transformations of biomass-derived compounds. *Chem Soc Rev* 43(3):765–778
36. Colmenares JC, Magdziarz A, Bielejewska A (2011) High-value chemicals obtained from selective photo-oxidation of glucose in the presence of nanostructured titanium photocatalysts. *Bioresour Technol* 102(24):11254–11257
37. Colmenares JC, Luque R, Campelo JM, Colmenares F, Karpinski Z, Romero AA (2009) Nanostructured photocatalysts and their applications in the photocatalytic transformation of lignocellulosic biomass: an overview. *Materials* 2(4):2228–2258
38. Zhang N, Zhang Y, Xu Y-J (2012) Recent progress on graphene-based photocatalysts: current status and future perspectives. *Nanoscale* 4(19):5792–5814
39. Zhang N, Liu S, Xu Y-J (2012) Recent progress on metal core@semiconductor shell nanocomposites as a promising type of photocatalyst. *Nanoscale* 4(7):2227–2238
40. Weng B, Liu S, Tang Z-R, Xu Y-J (2014) One-dimensional nanostructure based materials for versatile photocatalytic applications. *RSC Adv* 4(25):12685–12700
41. Liu S, Zhang N, Tang Z-R, Xu Y-J (2012) Synthesis of one-dimensional CdS@TiO₂ core-shell nanocomposites photocatalyst for selective redox: the dual role of TiO₂ shell. *ACS Appl Mater Interfaces* 4(11):6378–6385
42. Zhang M, Wang Q, Chen C, Zang L, Ma W, Zhao J (2009) Oxygen atom transfer in the photocatalytic oxidation of alcohols by TiO₂: oxygen isotope studies. *Angew Chem Int Ed* 48(33):6081–6084
43. Qu Y, Duan X (2013) Progress, challenge and perspective of heterogeneous photocatalysts. *Chem Soc Rev* 42(7):2568–2580
44. Kisch H (2013) Semiconductor photocatalysis-mechanistic and synthetic aspects. *Angew Chem Int Ed* 52(3):812–847
45. Yang M-Q, Zhang N, Pagliaro M, Xu Y-J (2014) Artificial photosynthesis over graphene–semiconductor composites. Are we getting better? *Chem Soc Rev* 43(24):8240–8254
46. Fan W, Zhang Q, Wang Y (2013) Semiconductor-based nanocomposites for photocatalytic H₂ production and CO₂ conversion. *Phys Chem Chem Phys* 15(8):2632–2649
47. Caron S, Dugger RW, Ruggeri SG, Ragan JA, Ripin DHB (2006) Large-scale oxidations in the pharmaceutical industry. *Chem Rev* 106(7):2943–2989
48. Fukuzumi S, Kishi T, Kotani H, Lee Y-M, Nam W (2011) Highly efficient photocatalytic oxygenation reactions using water as an oxygen source. *Nat Chem* 3(1):38–41
49. Ohkubo K, Kobayashi T, Fukuzumi S (2011) Direct oxygenation of benzene to phenol using quinolinium ions as homogeneous photocatalysts. *Angew Chem* 123(37):8811–8814
50. Ye X, Cui Y, Qiu X, Wang X (2014) Selective oxidation of benzene to phenol by Fe-CN/TS-1 catalysts under visible light irradiation. *Appl Catal B* 152:383–389
51. Zhang G, Yi J, Shim J, Lee J, Choi W (2011) Photocatalytic hydroxylation of benzene to phenol over titanium oxide entrapped into hydrophobically modified siliceous foam. *Appl Catal B* 102(1):132–139
52. Zheng Z, Huang B, Qin X, Zhang X, Dai Y, Whangbo M-H (2011) Facile in situ synthesis of visible-light plasmonic photocatalysts M@TiO₂ (M = Au, Pt, Ag) and evaluation of their photocatalytic oxidation of benzene to phenol. *J Mater Chem* 21(25):9079–9087
53. Chen J, Eberlein L, Langford CH (2002) Pathways of phenol and benzene photooxidation using TiO₂ supported on a zeolite. *J Photochem Photobiol A: Chem* 148(1):183–189
54. Bui TD, Kimura A, Ikeda S, Matsumura M (2010) Determination of oxygen sources for oxidation of benzene on TiO₂ photocatalysts in aqueous solutions containing molecular oxygen. *J Am Chem Soc* 132(24):8453–8458

55. Chen X, Zhang J, Fu X, Antonietti M, Wang X (2009) Fe-g-C₃N₄-catalyzed oxidation of benzene to phenol using hydrogen peroxide and visible light. *J Am Chem Soc* 131 (33):11658–11659
56. Shiraishi Y, Saito N, Hirai T (2005) Adsorption-driven photocatalytic activity of mesoporous titanium dioxide. *J Am Chem Soc* 127(37):12820–12822
57. Herron N, Tolman CA (1987) A highly selective zeolite catalyst for hydrocarbon oxidation. A completely inorganic mimic of the alkane. omega.-hydroxylases. *J Am Chem Soc* 109 (9):2837–2839
58. Izumi I, Dunn WW, Wilbourn KO, Fan F-RF, Bard AJ (1980) Heterogeneous photocatalytic oxidation of hydrocarbons on platinized titanium dioxide powders. *J Phys Chem* 84 (24):3207–3210
59. Fujihira M, Satoh Y, Osa T (1981) Heterogeneous photocatalytic oxidation of aromatic compounds on TiO₂. *Nature* 293:206–208
60. Shimizu K-I, Kaneko T, Fujishima T, Kodama T, Yoshida H, Kitayama Y (2002) Selective oxidation of liquid hydrocarbons over photoirradiated TiO₂ pillared clays. *Appl Catal A Gen* 225(1):185–191
61. López-Tenllado FJ, Marinas A, Urbano FJ, Colmenares JC, Hidalgo MC, Marinas JM, Moreno JM (2012) Selective photooxidation of alcohols as test reaction for photocatalytic activity. *Appl Catal B* 128:150–158
62. Lykakis IN, Tanielian C, Seghrouchni R, Orfanopoulos M (2007) Mechanism of decatungstate photocatalyzed oxygenation of aromatic alcohols: part II. Kinetic isotope effects studies. *J Mol Catal A: Chem* 262(1):176–184
63. Tanaka A, Hashimoto K, Kominami H (2012) Preparation of Au/CeO₂ exhibiting strong surface plasmon resonance effective for selective or chemoselective oxidation of alcohols to aldehydes or ketones in aqueous suspensions under irradiation by green light. *J Am Chem Soc* 134(35):14526–14533
64. Shishido T, Miyatake T, Teramura K, Hitomi Y, Yamashita H, Tanaka T (2009) Mechanism of photooxidation of alcohol over Nb₂O₅. *J Phys Chem C* 113(43):18713–18718
65. Higashimoto S, Kitao N, Yoshida N, Sakura T, Azuma M, Ohue H, Sakata Y (2009) Selective photocatalytic oxidation of benzyl alcohol and its derivatives into corresponding aldehydes by molecular oxygen on titanium dioxide under visible light irradiation. *J Catal* 266 (2):279–285
66. Higashimoto S, Suetsugu N, Azuma M, Ohue H, Sakata Y (2010) Efficient and selective oxidation of benzylic alcohol by O₂ into corresponding aldehydes on a TiO₂ photocatalyst under visible light irradiation: effect of phenyl-ring substitution on the photocatalytic activity. *J Catal* 274(1):76–83
67. Higashimoto S, Okada K, Azuma M, Ohue H, Terai T, Sakata Y (2012) Characteristics of the charge transfer surface complex on titanium (IV) dioxide for the visible light induced chemoselective oxidation of benzyl alcohol. *RSC Adv* 2(2):669–676
68. Li C-J, Xu G-R, Zhang B, Gong JR (2012) High selectivity in visible-light-driven partial photocatalytic oxidation of benzyl alcohol into benzaldehyde over single-crystalline rutile TiO₂ nanorods. *Appl Catal B* 115:201–208
69. Tsukamoto D, Shiraishi Y, Sugano Y, Ichikawa S, Tanaka S, Hirai T (2012) Gold nanoparticles located at the interface of anatase/rutile TiO₂ particles as active plasmonic photocatalysts for aerobic oxidation. *J Am Chem Soc* 134(14):6309–6315
70. Tanaka A, Hashimoto K, Kominami H (2011) Selective photocatalytic oxidation of aromatic alcohols to aldehydes in an aqueous suspension of gold nanoparticles supported on cerium (iv) oxide under irradiation of green light. *Chem Commun* 47(37):10446–10448
71. Li X, Weng B, Zhang N, Xu Y-J (2014) In situ synthesis of hierarchical In₂S₃-graphene nanocomposite photocatalyst for selective oxidation. *RSC Adv* 4(110):64484–64493
72. Zhang Y, Tang Z-R, Fu X, Xu Y-J (2011) Engineering the unique 2D mat of graphene to achieve graphene-TiO₂ nanocomposite for photocatalytic selective transformation: what

- advantage does graphene have over its forebear carbon nanotube? *ACS Nano* 5 (9):7426–7435
73. Zhang N, Yang M-Q, Tang Z-R, Xu Y-J (2014) Toward improving the graphene-semiconductor composite photoactivity via the addition of metal ions as generic interfacial mediator. *ACS Nano* 8(1):623–633
 74. Zhang N, Zhang Y, Pan X, Yang M-Q, Xu Y-J (2012) Constructing ternary CdS-graphene-TiO₂ hybrids on the flatland of graphene oxide with enhanced visible-light photoactivity for selective transformation. *J Phys Chem C* 116(34):18023–18031
 75. Zhang N, Zhang Y, Pan X, Fu X, Liu S, Xu Y-J (2011) Assembly of CdS nanoparticles on the two-dimensional graphene scaffold as visible-light-driven photocatalyst for selective organic transformation under ambient conditions. *J Phys Chem C* 115(47):23501–23511
 76. Han C, Yang M-Q, Zhang N, Xu Y-J (2014) Enhancing the visible light photocatalytic performance of ternary CdS-(graphene-Pd) nanocomposites via a facile interfacial mediator and co-catalyst strategy. *J Mater Chem A* 2(45):19156–19166
 77. Zhang N, Fu X, Xu Y-J (2011) A facile and green approach to synthesize Pt@CeO₂ nanocomposite with tunable core-shell and yolk-shell structure and its application as a visible light photocatalyst. *J Mater Chem* 21(22):8152–8158
 78. Zhang N, Liu S, Fu X, Xu Y-J (2011) A simple strategy for fabrication of “Plum-Pudding” type Pd@CeO₂ semiconductor nanocomposite as a visible-light-driven photocatalyst for selective oxidation. *J Phys Chem C* 115(46):22901–22909
 79. Kesavan L, Tiruvalam R, Ab Rahim MH, bin Saiman MI, Enache DI, Jenkins RL, Dimitratos N, Lopez-Sanchez JA, Taylor SH, Knight DW (2011) Solvent-free oxidation of primary carbon-hydrogen bonds in toluene using Au-Pd alloy nanoparticles. *Science* 331(6014):195–199
 80. Yuan R, Fan S, Zhou H, Ding Z, Lin S, Li Z, Zhang Z, Xu C, Wu L, Wang X (2013) Chlorine-radical-mediated photocatalytic activation of C–H bonds with visible light. *Angew Chem* 125(3):1069–1073
 81. Sarina S, Zhu H, Zheng Z, Bottle S, Chang J, Ke X, Zhao J-C, Huang Y, Sutrisno A, Willans M (2012) Driving selective aerobic oxidation of alkyl aromatics by sunlight on alcohol grafted metal hydroxides. *Chem Sci* 3(6):2138–2146
 82. Zhang Y, Zhang N, Tang Z-R, Xu Y-J (2012) Transforming CdS into an efficient visible light photocatalyst for selective oxidation of saturated primary C–H bonds under ambient conditions. *Chem Sci* 3(9):2812–2822
 83. Yang M-Q, Zhang Y, Zhang N, Tang Z-R, Xu Y-J (2013) Visible-light-driven oxidation of primary C–H bonds over CdS with dual Co-catalysts graphene and TiO₂. *Sci Rep* 3:3314
 84. Ohno T, Masaki Y, Hirayama S, Matsumura M (2001) TiO₂-photocatalyzed epoxidation of 1-decene by H₂O₂ under visible light. *J Catal* 204(1):163–168
 85. Christopher P, Xin H, Linic S (2011) Visible-light-enhanced catalytic oxidation reactions on plasmonic silver nanostructures. *Nat Chem* 3(6):467–472
 86. Marimuthu A, Zhang J, Linic S (2013) Tuning selectivity in propylene epoxidation by plasmon mediated photo-switching of Cu oxidation state. *Science* 339(6127):1590–1593
 87. Zhang Y, Zhang N, Tang Z-R, Xu Y-J (2012) Graphene transforms wide band gap ZnS to VIS photocatalyst. -Macromolecular Photosensitizer. *ACS Nano* 6(11):9777–9789
 88. Otsuki S, Nonaka T, Takashima N, Qian W, Ishihara A, Imai T, Kabe T (2000) Oxidative desulfurization of light gas oil and vacuum gas oil by oxidation and solvent extraction. *Energ Fuel* 14(6):1232–1239
 89. Wojaczynska E, Wojaczynski J (2010) Enantioselective synthesis of sulfoxides: 2000–2009. *Chem Rev* 110(7):4303–4356
 90. Bonesi SM, Fagnoni M, Albini A (2008) Biaryl formation involving carbon-based leaving groups: why not? *Angew Chem Int Ed* 47(52):10022–10025
 91. Baciocchi E, Giacco TD, Elisei F, Gerini MF, Guerra M, Lapi A, Liberali P (2003) Electron transfer and singlet oxygen mechanisms in the photooxygenation of dibutyl sulfide and thioanisole in MeCN sensitized by N-methylquinolinium tetrafluoroborate and

- 9, 10-dicyanoanthracene. The probable involvement of a thiadioxirane intermediate in electron transfer photooxygenations. *J Am Chem Soc* 125(52):16444–16454
92. Liang J, Gu C, Kacher M, Foote CS (1983) Chemistry of singlet oxygen. 45. Mechanism of the photooxidation of sulfides. *J Am Chem Soc* 105(14):4717–4721
93. Nahm K, Foote CS (1989) Trimethyl phosphite traps intermediates in the reaction of singlet oxygen (102) and diethyl sulfide. *J Am Chem Soc* 111(5):1909–1910
94. Nahm K, Li Y, Evanseck JD, Houk K, Foote CS (1993) Structures and energies of intermediates in the reactions of singlet oxygen with organic phosphines and sulfides. *J Am Chem Soc* 115(11):4879–4884
95. Lang X, Leow WR, Zhao J, Chen X (2015) Synergistic photocatalytic aerobic oxidation of sulfides and amines on TiO₂ under visible-light irradiation. *Chem Sci* 6(2):1075–1082
96. Company A, Sabenya G, González-Béjar M, Gómez L, Clémancey M, Blondin G, Jasniewski AJ, Puri M, Browne WR, Latour J-M (2014) Triggering the generation of an iron (IV)-oxo compound and its reactivity toward sulfides by RuII photocatalysis. *J Am Chem Soc* 136(12):4624–4633
97. Gu X, Li X, Chai Y, Yang Q, Li P, Yao Y (2013) A simple metal-free catalytic sulfoxidation under visible light and air. *Green Chem* 15(2):357–361
98. Li X-H, Chen J-S, Wang X, Sun J, Antonietti M (2011) Metal-free activation of dioxygen by graphene/g-C₃N₄ nanocomposites: functional dyads for selective oxidation of saturated hydrocarbons. *J Am Chem Soc* 133(21):8074–8077
99. Liu S, Yang M-Q, Tang Z-R, Xu Y-J (2014) A nanotree-like CdS/ZnO nanocomposite with spatially branched hierarchical structure for photocatalytic fine-chemical synthesis. *Nano-scale* 6(13):7193–7198
100. Liu S, Chen Z, Zhang N, Tang Z-R, Xu Y-J (2013) An efficient self-assembly of CdS nanowires-reduced graphene oxide nanocomposites for selective reduction of nitro organics under visible light irradiation. *J Phys Chem C* 117(16):8251–8261
101. Yang M-Q, Pan X, Zhang N, Xu Y-J (2013) A facile one-step way to anchor noble metal (Au, Ag, Pd) nanoparticles on a reduced graphene oxide mat with catalytic activity for selective reduction of nitroaromatic compounds. *CrystEngComm* 15(34):6819–6828
102. Yang M-Q, Weng B, Xu Y-J (2013) Improving the visible light photoactivity of In₂S₃-graphene nanocomposite via a simple surface charge modification approach. *Langmuir* 29(33):10549–10558
103. Brezova V, Blažková A, Šurina I, Havlinova B (1997) Solvent effect on the photocatalytic reduction of 4-nitrophenol in titanium dioxide suspensions. *J Photochem Photobiol A: Chem* 107(1):233–237
104. Xu C, Yuan Y, Yuan R, Fu X (2013) Enhanced photocatalytic performances of TiO₂-graphene hybrids on nitro-aromatics reduction to amino-aromatics. *RSC Adv* 3(39):18002–18008
105. Chen Z, Liu S, Yang M-Q, Xu Y-J (2013) Synthesis of uniform CdS nanospheres/graphene hybrid nanocomposites and their application as visible light photocatalyst for selective reduction of nitro organics in water. *ACS Appl Mater Interfaces* 5(10):4309–4319
106. Yuan L, Yang M-Q, Xu Y-J (2014) A low-temperature and one-step method for fabricating ZnIn₂S₄-GR nanocomposites with enhanced visible light photoactivity. *J Mater Chem A* 2(35):14401–14412
107. Liu S, Yang M-Q, Xu Y-J (2014) Surface charge promotes the synthesis of large, flat structured graphene-(CdS nanowire)-TiO₂ nanocomposites as versatile visible light photocatalysts. *J Mater Chem A* 2(2):430–440
108. Han C, Chen Z, Zhang N, Colmenares JC, Xu Y-J (2015) Hierarchically CdS decorated 1D ZnO nanorods-2D graphene hybrids: low temperature synthesis and enhanced photocatalytic performance. *Adv Funct Mater* 25(2):221–229
109. Zhang N, Xu Y-J (2013) Aggregation- and leaching-resistant, reusable, and multifunctional Pd@CeO₂ as a robust nanocatalyst achieved by a hollow core-shell strategy. *Chem Mater* 25(9):1979–1988

110. Ohtani B, Tsuru S, Nishimoto S, Kagiya T, Izawa K (1990) Photocatalytic one-step syntheses of cyclic imino acids by aqueous semiconductor suspensions. *J Org Chem* 55(21):5551–5553
111. Ohtani B, Kawaguchi J, Kozawa M, Nakaoka Y, Nosaka Y, Nishimoto S (1995) Effect of platinum loading on the photocatalytic activity of cadmium(II) sulfide particles suspended in aqueous amino acid solutions. *J Photochem Photobiol A: Chem* 90(1):75–80
112. Ohtani B, Iwai K, Kominami H, Matsuura T, Kera Y, Nishimoto S-i (1995) Titanium (IV) oxide photocatalyst of ultra-high activity for selective N-cyclization of an amino acid in aqueous suspensions. *Chem Phys Lett* 242(3):315–319
113. Nishimoto S, Ohtani B, Yoshikawa T, Kagiya T (1983) Photocatalytic conversion of primary amines to secondary amines and cyclization of polymethylene- α , ω -diamines by an aqueous suspension of titanium (IV) oxide/platinum. *J Am Chem Soc* 105(24):7180–7182
114. Ohtani B, Osaki H, Nishimoto S, Kagiya T (1986) A novel photocatalytic process of amine N-alkylation by platinized semiconductor particles suspended in alcohols. *J Am Chem Soc* 108(2):308–310
115. Ohtani B, Goto Y, Nishimoto S-I, Inui T (1996) Photocatalytic transfer hydrogenation of Schiff bases with propan-2-ol by suspended semiconductor particles loaded with platinum deposits. *J Chem Soc, Faraday Trans* 92(21):4291–4295
116. Zhao J, Zheng Z, Bottle S, Chou A, Sarina S, Zhu H (2013) Highly efficient and selective photocatalytic hydroamination of alkynes by supported gold nanoparticles using visible light at ambient temperature. *Chem Commun* 49(26):2676–2678
117. Gonzalez-Bejar M, Peters K, Hallett-Tapley GL, Grenier M, Scaiano JC (2013) Rapid one-pot propargylamine synthesis by plasmon mediated catalysis with gold nanoparticles on ZnO under ambient conditions. *Chem Commun* 49(17):1732–1734
118. Caronna T, Gambarotti C, Palmisano L, Punta C, Recupero F (2003) Sunlight induced functionalisation of some heterocyclic bases in the presence of polycrystalline TiO₂. *Chem Commun* 18:2350–2351
119. Caronna T, Gambarotti C, Palmisano L, Punta C, Recupero F (2005) Sunlight-induced reactions of some heterocyclic bases with ethers in the presence of TiO₂: a green route for the synthesis of heterocyclic aldehydes. *J Photochem Photobiol A: Chem* 171(3):237–242
120. Rueping M, Zoller J, Fabry DC, Poschary K, Koenigs RM, Weirich TE, Mayer J (2012) Light-mediated heterogeneous cross dehydrogenative coupling reactions: metal oxides as efficient, recyclable, photoredox catalysts in C–C bond forming reactions. *Chem –Eur J* 18(12):3478–3481
121. Möhlmann L, Baar M, Rieß J, Antonietti M, Wang X, Blechert S (2012) Carbon nitride-catalyzed photoredox C–C bond formation with N-aryltetrahydroisoquinolines. *Adv Synth Catal* 354(10):1909–1913